Supporting Information

Ameliorating Defects in Wide Bandgap Tin Perovskite Solar Cells Using Fluorinated Solvent and Hydrazide

Dhruba B. Khadka[1]*, Yasuhiro Shirai[1], Ryoji Sahara[2], Masatoshi Yanagida[1], and Kenjiro Miyano[1]

[1]Photovoltaic Materials Group, Center for GREEN Research on Energy and Environmental Materials, National Institute for Materials Science (NIMS), 1-1 Namiki, Tsukuba, Ibaraki 305-0044, Japan
[2]Computational Structural Materials Group, Research Center for Structural Materials, National Institute for Materials Science (NIMS), 1-2-1, Sengen, Tsukuba, Ibaraki 305-0047, Japan
Corresponding Author
*E-mail: KHADKA.B.Dhruba@nims.go.jp

Table and Figures

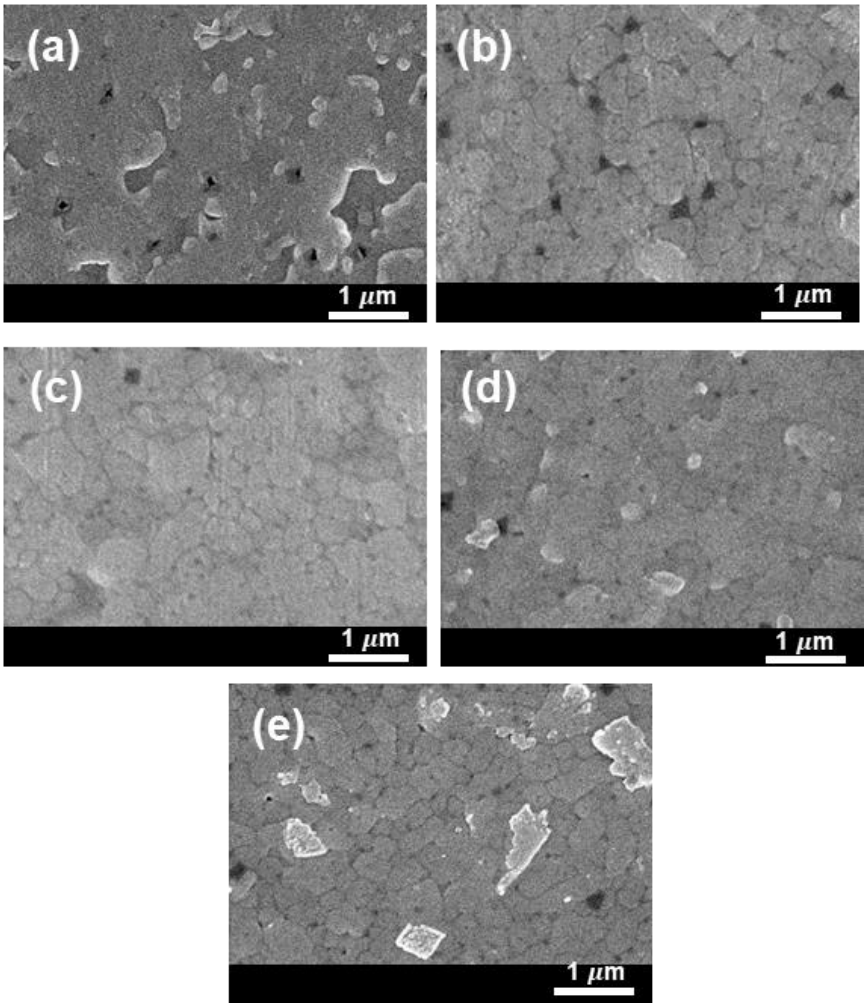

Figure S1. SEM images of WB-Sn-HP films with surface treatment using different F-BHZ precursor concentrations; a) control, b) 0.5 mg/ml, c) 1 mg/ml, d) 1.5 mg/ml, and e) 2 mg/ml, respectively.

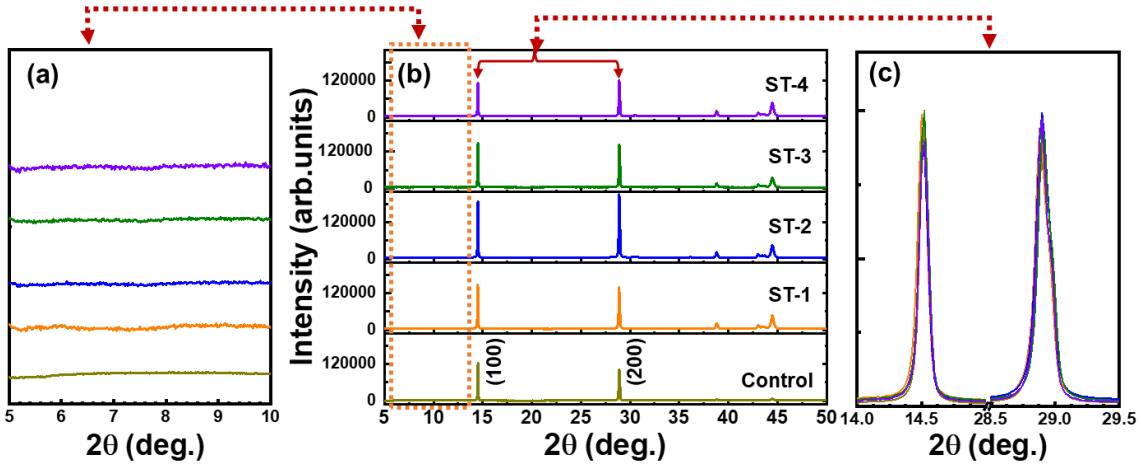

Figure S2. XRD patterns of WB-Sn-HP films [0 mg/ml (control), 0.5 mg/ml (ST-1), 1 mg/ml (ST-2), 1.5 mg/ml (ST-3), and 2 mg/ml (ST-4)]. a) XRD patterns zoomed-in $2\theta<10^{o}$). b) XRD patterns of full 2θ range. c) Normalized XRD patterns zoomed in dominant peaks (100) and (200).

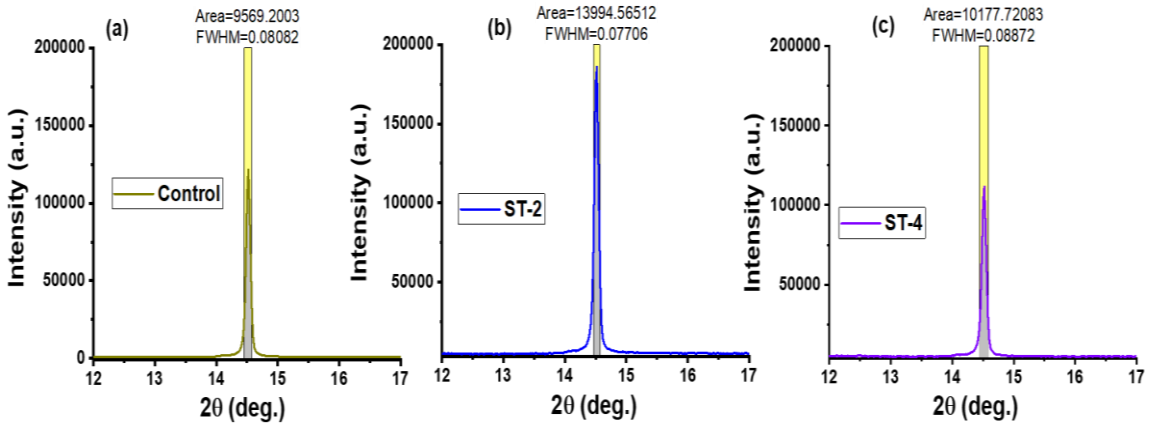

Figure S3. FWHM of WB-Sn-HP films; (a) control, (b) ST-2 (1 mg/ml), and (c) ST-4 (2mg/ml).

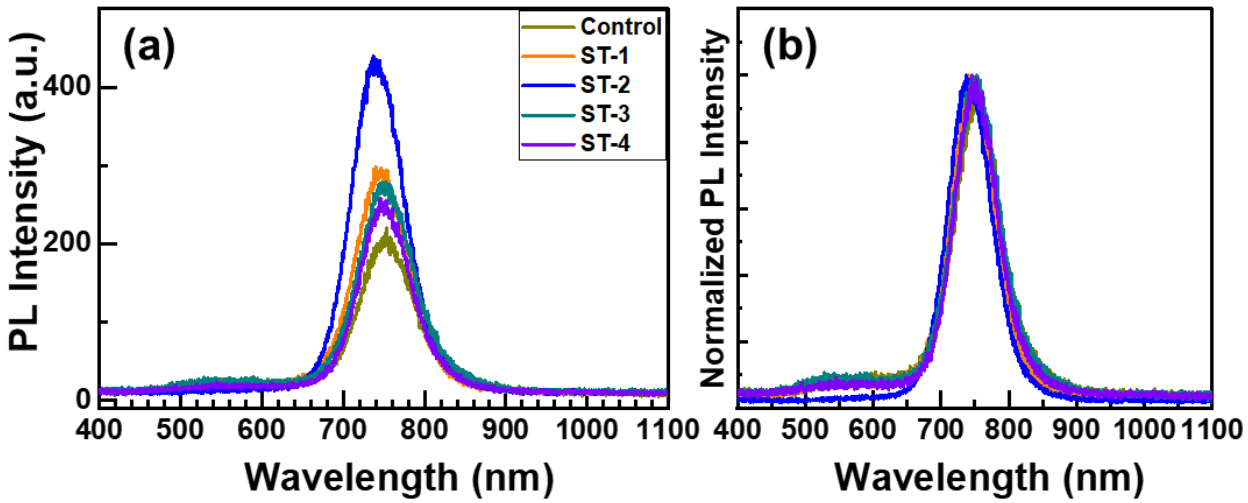

Figure S4. a) PL spectra of WB-Sn-HP films with F-BHZ treatment (0-2 mg; control, ST-1 (0.5 mg/ml), ST-2 (1 mg/ml), ST-3 (1.5 mg/ml), ST-4 (2 mg/ml) on ITO substrates (ITO/Sn-HP). b) Normalized PL spectra.

Table S1. Summarized device parameters of the WB-Sn-PSCs (control and ST devices). The tabulated data present the best device parameters, the average value, and the standard deviation (SD) (20 devices from 4 batches).

F-BHZ (mg/ml)	J_{SC} (mA cm^{-2})	V_{OC} (V)	*FF*	*PCE* (%)	PCE (average ± SD)
0	12.58	0.914	0.692	7.96	7.09 ± 0.41
	12.76	0.928	0.622	7.37	
0.5	14.12	0.958	0.722	9.77	8.48 ± 0.56
	14.24	0.946	0.662	8.92	
1	14.37	1.024	0.757	11.14	10.58 ± 0.39
	14.465	1.036	0.696	10.43	
1.5	13.78	1.014	0.736	10.28	9.62 ± 0.36
	14.465	0.994	0.684	9.84	
2	12.83	0.956	0.714	8.75	8.22 ± 0.37
	13.37	0.976	0.676	8.82	

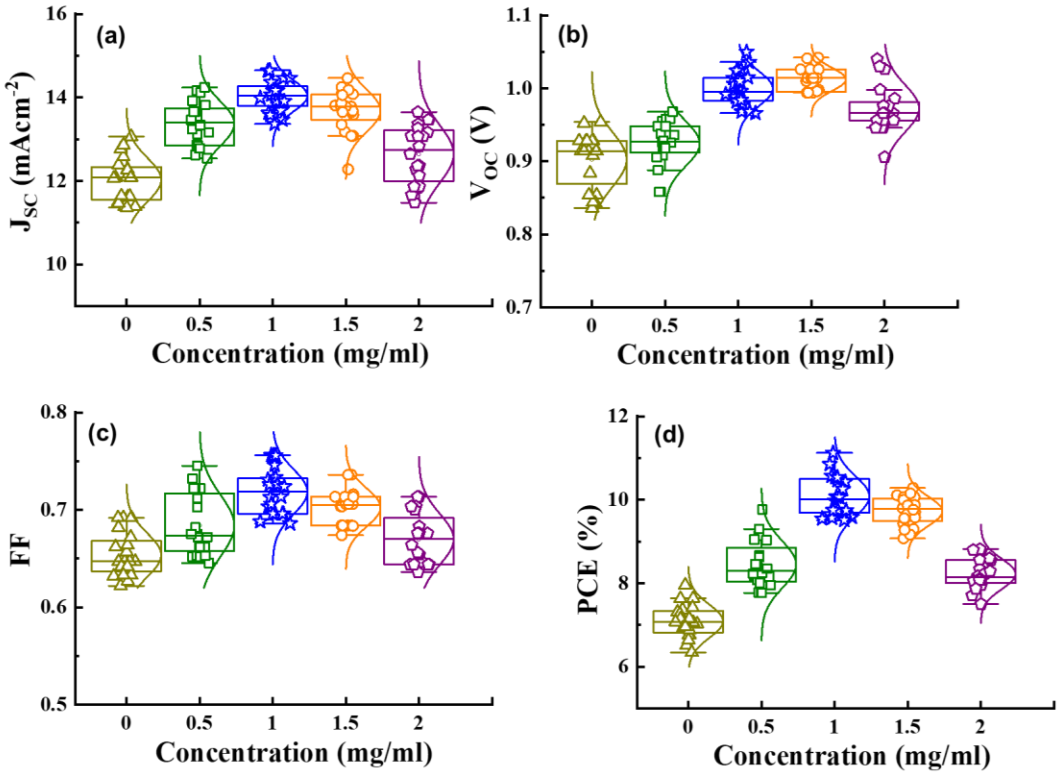

Figure S5. Statistics of device parameters for the WB-Sn-PSCs with control and ST (0.5-2 mg/ml; F-BHZ) films. Histogram of device parameters: (a) J_{SC}, (b) V_{OC}, (c) *FF*, and (d) PCE of 20-PSC devices fabricated in 4 different batches.

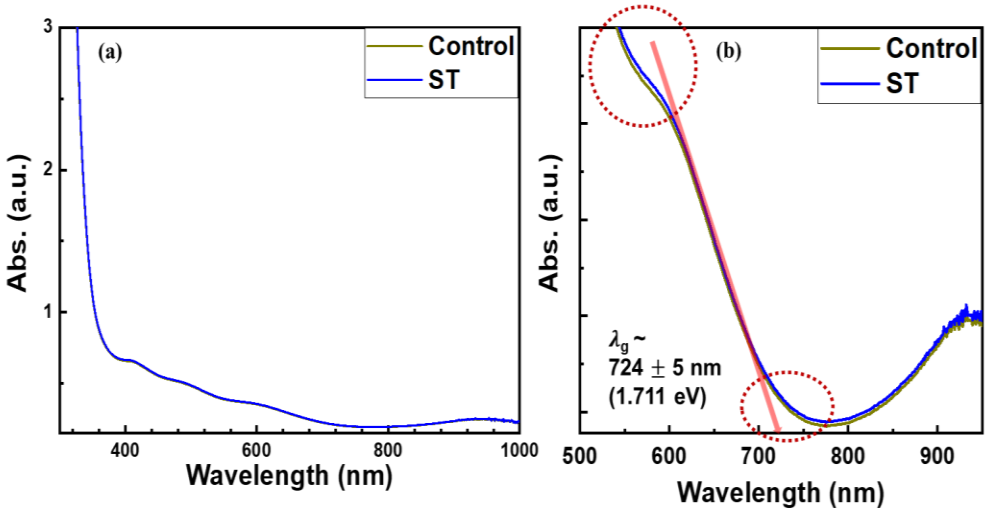

Figure S6. (a) absorption spectra and (b) absorption spectra zoom at the band gap edge of the control and F-BHZ-treated wide bandgap tin perovskite films. The encircled regions highlight the change in absorption spectra.

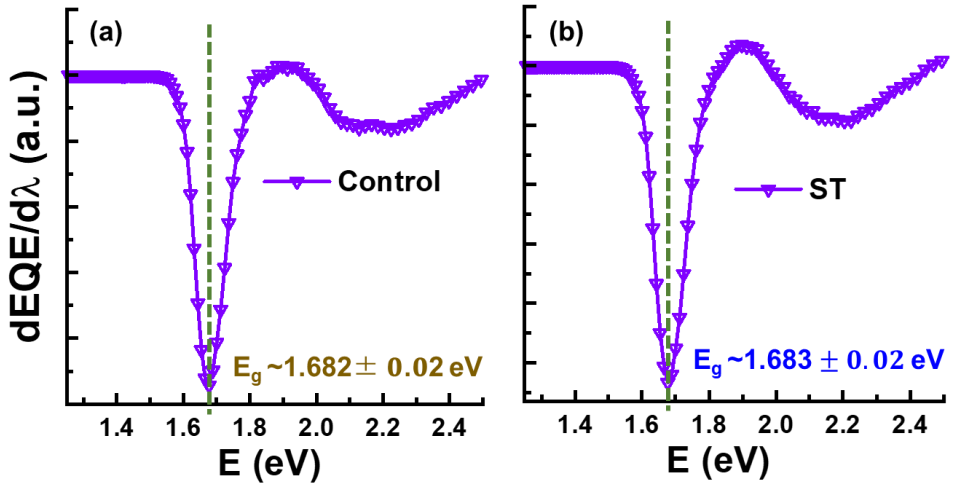

Figure S7. Bandgap energy of WB-Sn-HP; (a) control and (b) ST calculated from the EQE spectra analysis.

Table S2. Summary of device reports on WB-Sn-perovskite (mixed cations/anions, functional additives, passivation, and interfacial layer).

Device structure	WB-Sn-HP	Method	Eg (eV)	J_{SC} ($mAcm^{-2}$)	V_{OC} (V)	FF	PCE (%)	date	Ref.
FTO/TiO_2/$MASnBr_3$/ P3HT/**Ag**	$MASnBr_3$	Co-evaporation	2.2	4.27	0.498	0.491	1.12	2016	[1]
ITO/PEDOT:PSS/Sn-HP/ICBA/Bphen/Ag	$FA_{0.55}MA_{0.25}Cs_{0.1}PMA_{0.1}SnBr_2I$	PMA mixed	1.93	8.804	0.975	71.12	6.2	2024	[2]
FTO/m/c-TiO_2/ Sn-HP/spiro-OMeTAD /**Au**	$MASnIBr_2$	Additive SnF_2	1.75	13.78	0.45	0.573	3.70	2017	[3]
ITO/PEDOT:PSS/Sn-HP/ /PCBM/PEI/**Au**	$FASnI_2Br$	Additive SnF_2	1.55	19.82	0.60	0.64	7.61	2020	[4]
ITO/PEDOT:PSS/Sn-HP/ICBA/BCP/**Ag**	$CsSnBr_3$	Additive SnF_2	1.79	13.96	0.37	0.594	3.04	2017	[5]
FTO/TiO_2/Al_2O_3/Sn-HP/**Carbon**	$CsSnIBr_2$	Additive HPA	1.63	17.4	0.35	0.55	3.20	2016	[6]
FTO/PEDOT:PSS/Sn-HP/ICBA/Bphen/**Ag**	$(FA,MA)SnI_2Br$	Interface KSCN	1.63	20.88	0.82	0.64	11.17	2022	[7]
ITO/PEDOT:PSS/Sn-HP/ICBA/BCP/**Ag**	$EDA(FAMA)SnI_2Br$	Interface 4F-BCl	1.63	13.41	0.94	0.86	11.03	2023	[8]
ITO/PEDOT:PSS/Sn-HP/ICBA/BCP/**Ag**	$GA_{0.06}(FA_{0.8}Cs_{0.2})_{0.94}SnI_2Br$	Additive GeI_2/EDABr$_2$	1.62	13.74	0.66	0.53	4.86	2022	[9]
FTO/PEDOT:PSS/Sn-HP/C_{60}/BCP/**Ag**	$GA_{0.06}(FA_{0.8}Cs_{0.2})_{0.94}SnI_2Br$	Bulk interface EDA	1.63	15.16	0.64	0.72	7.50	2021	[9]
ITO/PEDOT:PSS/Sn-HP/ETL/**Ag**	$PEA_{0.15}FA_{0.75}MA_{0.1}SnI_2Br$	Additive PEABr	1.66	16.89	0.67	0.703	7.96	2022	[10]
ITO/PEDOT:PSS/2PACz/Sn-HP/C_{60}/BCP/**Ag**	$EDA_{0.01}(GA_{0.06}(FA_{0.8}Cs_{0.2})_{0.94})_{0.98}SnI_2Br$	HTL interface	1.62	16.22	0.74	0.73	8.66	2022	[11]
ITO/PEDOT:PSS/Sn-HP/ICBA/BCP/**Ag**	$PEA_{0.15}FA_{0.75}MA_{0.1}SnI_2Br$	Bulk interface F-BHZ	1.68	14.37	1.024	0.757	11.14	2024	This work

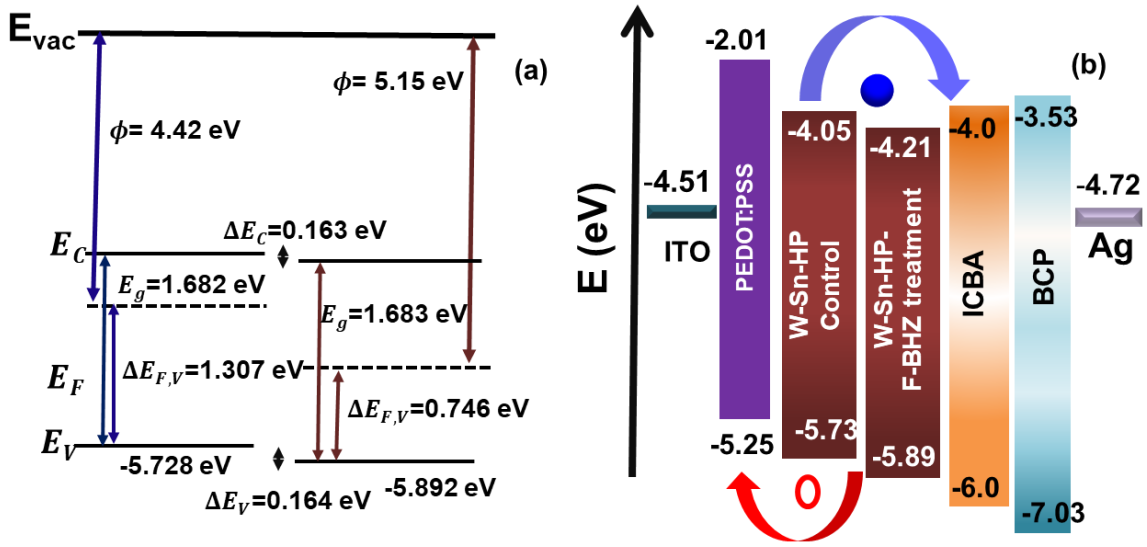

Figure S8. Schematic illustration: a) Energy levels constructed from UPS data (Fig. 3a-d). b) Energy band diagram of WB-Sn-PSC extracted from experimental results.

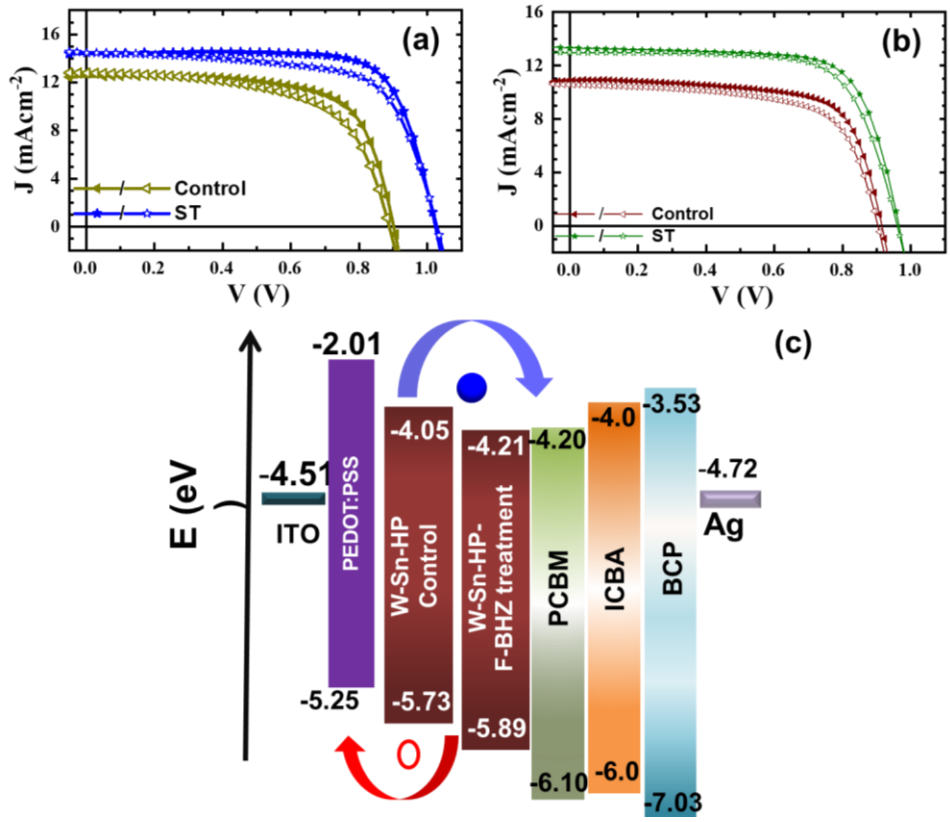

Figure S9. (a) J-V results of WB-Sn-PSCs with ICBA and PCBM as ETL. Here, filled/unfilled symbols stand for forward/reverse scan direction. Energy band diagram of WB-Sn-PSC with ETL: PCBM and ICBA.

Table R3. Summary of device parameters of the WB-Sn-PSCs (control and ST) with ICBA and PCBM as ETL.

Device structure:		ITO/PEDOT:PSS/WB-Sn-HP/**ICBA**/BCP/Ag				ITO/PEDOT: PSS/WB-Sn-HP/**PCBM**/BCP/Ag			
Device	Scan direction	J_{SC} ($mAcm^{-2}$)	V_{OC} (V)	FF	PCE (%)	J_{SC} ($mAcm^{-2}$)	V_{OC} (V)	FF	PCE (%)
Control	F	12.58	0.914	0.692	7.96	10.77	0.851	0.697	6.39
	R	12.76	0.928	0.622	7.37	11.16	0.863	0.656	6.32
ST	F	14.37	1.024	0.757	11.14	12.95	0.959	0.717	8.90
	R	14.46	1.036	0.696	10.43	13.41	0.967	0.706	9.15

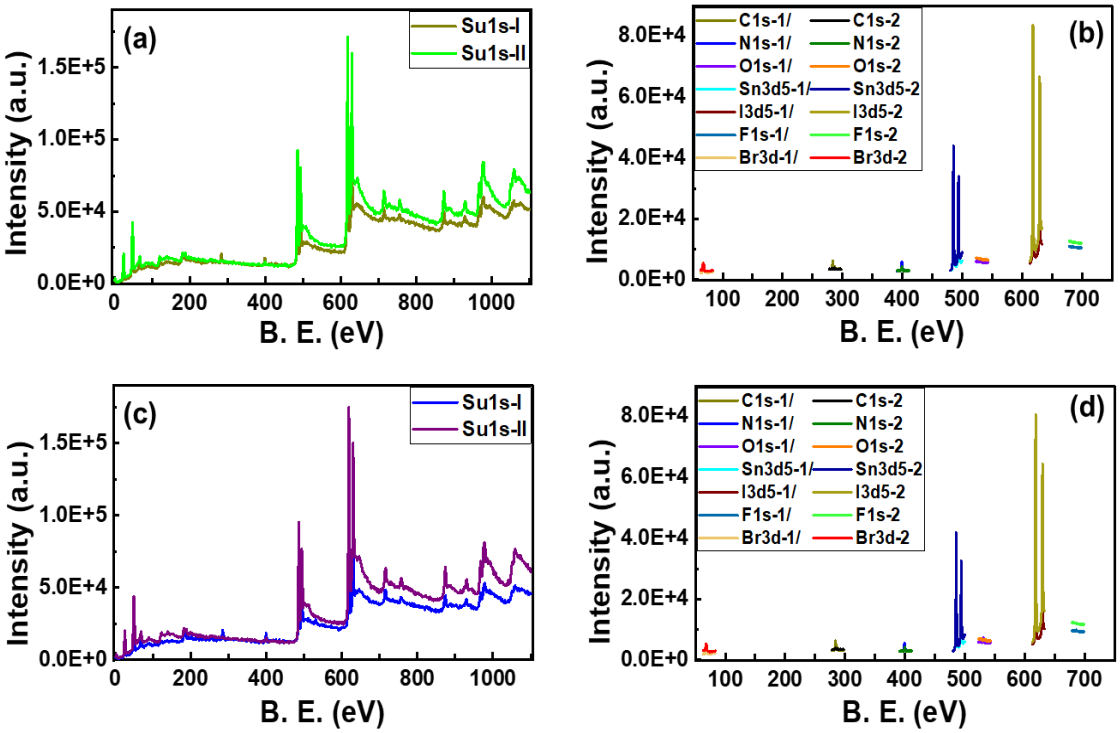

Figure S10. XPS survey and individual spectra of WB-Sn-HP films; (a, b) control and (c, d) FHZ additive. 1st and 2nd spectra represent spectra obtained from the film surface and depth, respectively.

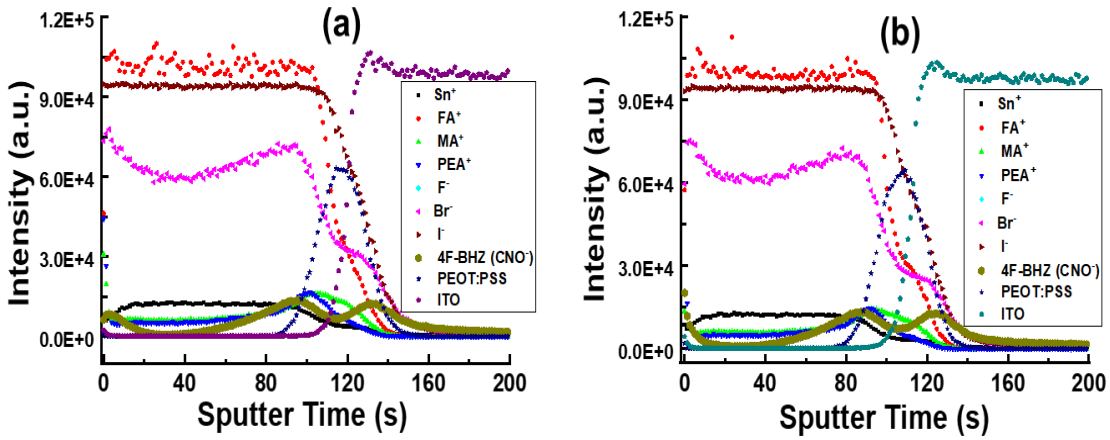

Figure S11. ToF-SIMS elemental depth profiles of the ITO/Sn-HP films; (a) control and (b) ST. There are selected ionic species; ITO (InO_2^-), PEDOT:PSS ($C_8H_7SO_3^-$), Sn-HP (Sn^+, FA^+, MA^+, PEA^+, F^-, Cl^-, Br^-, I^-, and IPL (4F-BHZ).

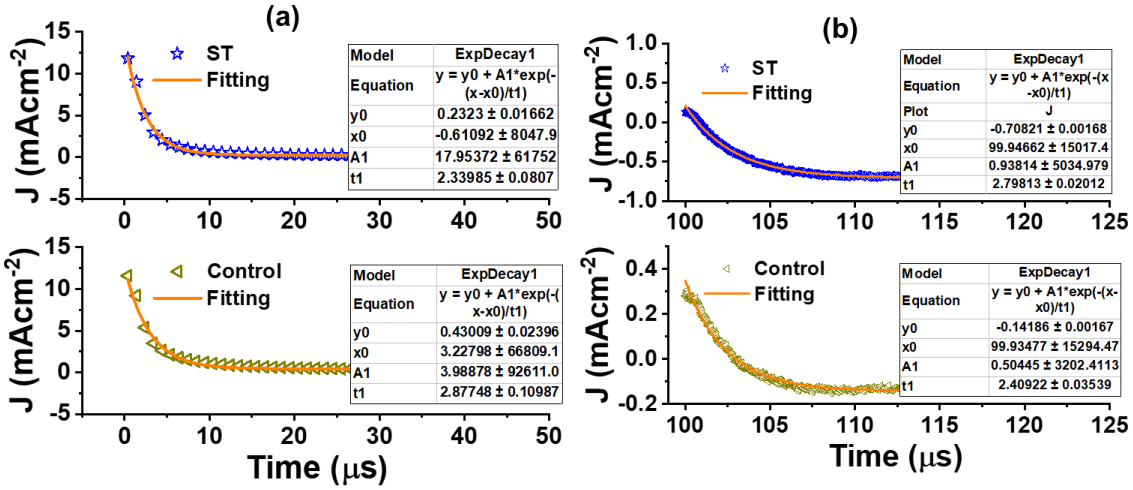

Figure S12. Fitting of TPC curves (Fig. 4b): a) regime I and b) regime II.

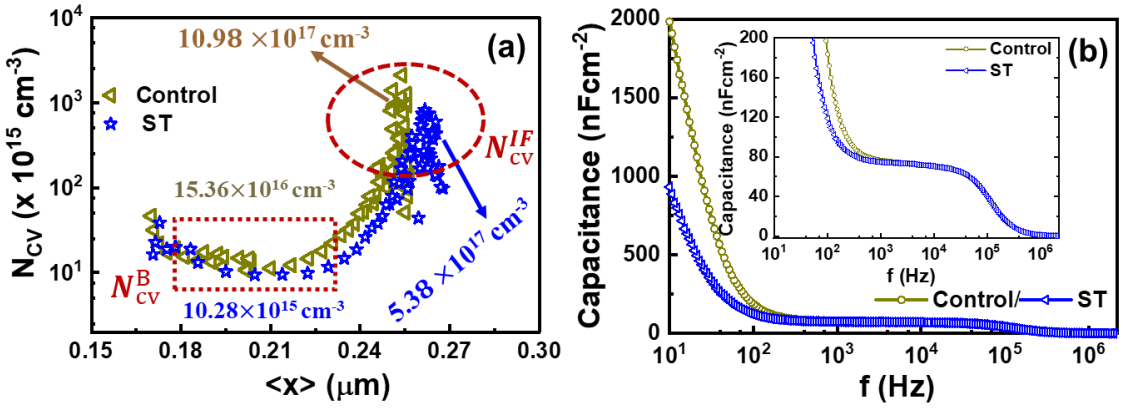

Figure S13. Admittance analysis of WB-Sn-PSCs; a) Carrier profile extracted from C–V curves. b) *C–f* spectra under illumination.

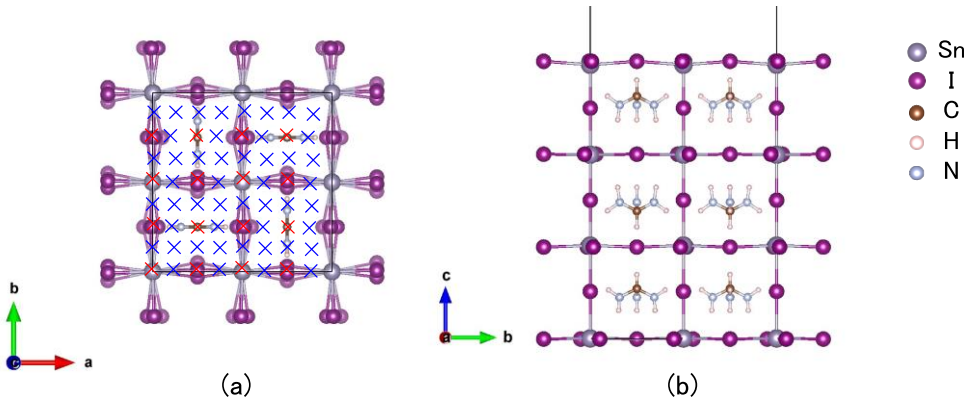

Figure S14. (a)Top and (b)side view of the SnI_2-terminated surface of the slab model 1. The blue and red colored × in Fig.(a) represent the initial adsorption side of the molecule.

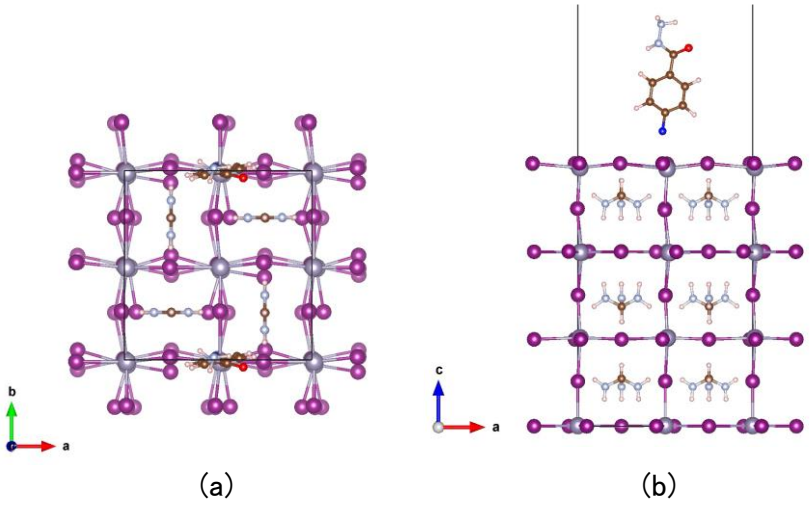

Figure S15. (a) Top view and (b) side view of the optimized structure of Model2, with the standing molecule on the side on the substrate as the initial position. The adsorption energy is -0.62 eV/system, and the F-Sn bond length is 2.78Å.

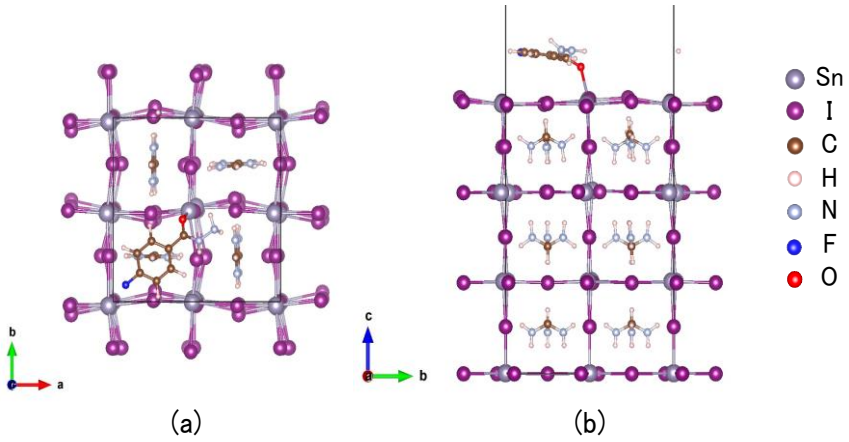

Figure S16. (a) Top view and (b) side view of the optimized structure of Model3, with the molecule laying on the back of the substrate as the initial position. The adsorption energy is -1.27 eV/system, and the O-Sn bond length is 2.41Å.

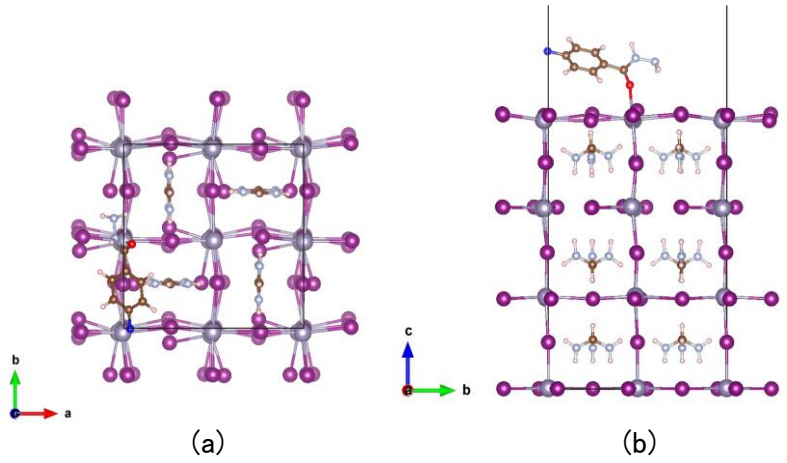

Figure S17. (a) Top view and (b) side view of the optimized structure of Model4, with the molecule laying on the side on the substrate as the initial position. The adsorption energy is -1.47 eV/system, and the O-Sn bond length is 2.34Å.

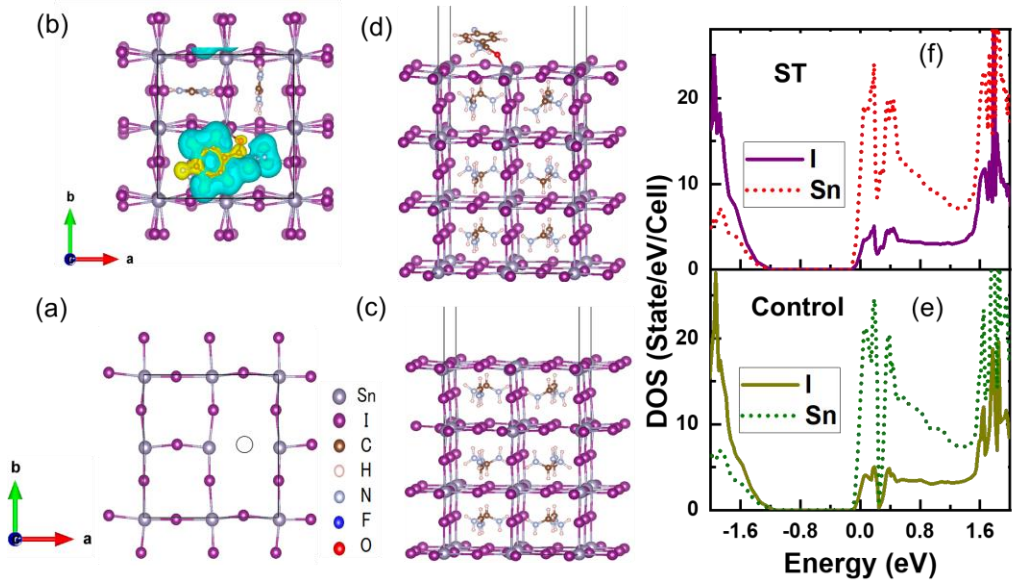

Figure S18. Top view of iodine vacancy model (a) and F-BHZ molecules laying on the surface and corresponding side view without (c) and with the molecule (d). The atom-projected density of states without (e) and with the molecule (f) for iodine vacancy defect surface. Where the Fermi energy is set at energy zero (at Fermi energy at CBM).

References

[1] M. Kaleli, E. Şen, H. E. Lapa, D. A. Aldemir, *Physica B Condens Matter* **2022**, *645*, 414293.

[2] C.-H. Kuan, Y.-C. Chen, S. Narra, C.-F. Chang, Y.-W. Tsai, J.-M. Lin, G.-R. Chen, E. W.-G. Diau, *ACS Energy Lett* **2024**, *9*, 2351.

[3] M. Xiao, S. Gu, P. Zhu, M. Tang, W. Zhu, R. Lin, C. Chen, W. Xu, T. Yu, J. Zhu, *Adv Opt Mater* **2018**, *6*,1700615.

[4] J. Zhang, J. Qin, T. Wu, B. Hu, *J Phys Chem Lett* **2020**, *11*, 6996.

[5] T. Bin Song, T. Yokoyama, C. C. Stoumpos, J. Logsdon, D. H. Cao, M. R. Wasielewski, S. Aramaki, M. G. Kanatzidis, *J Am Chem Soc* **2017**, *139*, 836.

[6] W. Li, J. Li, J. Li, J. Fan, Y. Mai, L. Wang, *J Mater Chem A* **2016**, *4*, 17104.

[7] J.-J. Cao, Y.-H. Lou, W.-F. Yang, K.-L. Wang, Z.-H. Su, J. Chen, C.-H. Chen, C. Dong, X.-Y. Gao, Z.-K. Wang, *Chem Eng J* **2022**, *433*, 133832.

[8] T.-Y. Teng, F. Hu, Y.-H. Lou, J.-J. Cao, C.-H. Chen, Y.-R. Shi, K.-L. Wang, J. Chen, Z.-K. Wang, L.-S. Liao, *Chem Eng J* **2023**, *457*, 141292.

[9] M. Chen, G. Kapil, Y. Li, M. A. Kamarudin, A. K. Baranwal, K. Nishimura, S. R. Sahamir, Y. Sanehira, H. Li, C. Ding, Z. Zhang, Q. Shen, S. Hayase, *J Power Sources* **2022**, *520*, 230848.

[10] S. Cho, P. Pandey, J. Park, T.-W. Lee, H. Ahn, H. Choi, D.-W. Kang, *Chem Eng J* **2022**, *446*, 137388.

[11] M. Chen, G. Kapil, L. Wang, S. Razey Sahamir, A. K. Baranwal, K. Nishimura, Y. Sanehira, Z. Zhang, M. Akmal Kamarudin, Q. Shen, S. Hayase, *Chem Eng J* **2022**, *436*, 135196.